Simulation of Gas-Surface Dynamical Interactions

Axel Groß

Abteilung Theoretische Chemie
Universität Ulm
Albert-Einstein-Allee 11
D-89069 Ulm
GERMANY

email: axel.gross@uni-ulm.de

Abstract

The interaction of atoms and molecule with surfaces is of great technological relevance. Both advantageous and harmful processes can occur at surfaces. If an atom or molecule impinges on a surface, it can either scatter back into the gas phase or become adsorbed on the surface. Molecules can furthermore undergo chemical reactions at the surface. All these processes are accompanied by energy transfer between the impinging projectile and the substrate.

The simulation of the dynamics of the gas-surface interaction still represents a considerable challenge since the coupling of a low-dimensional object, the impinging atom or molecule, to the substrate with in principle infinitely many degrees of freedom has to be modeled. Furthermore, depending on the mass of the atom or molecule, quantum effects both in the molecular motion as well as in the excitation of the substrate have to be taken into account. In this lecture, the quantum and classical methods required for the simulation of gas-surface dynamical interactions will be reviewed. Furthermore, the main processes occuring in the interaction of atoms and molecules with substrates will be illustrated using quantum calculations and classical molecular dynamics simulations.

1   Introduction

Understanding the interaction of atoms and molecules with surfaces plays an important role in a wide range of technologically relevant applications [1]. Among those are the *heterogenous catalysis* – the majority of reactions in the chemical industry employ catalysts; *crystal growth*, which determines, e.g., the quality of semiconductor devices; *corrosion* and *lubrication*, which influences the durability of mechanical systems; or *friction*, which determines the energy transfer to surfaces, as for example in the interaction between the atmosphere and rockets or high-speed missiles which causes significant temperature rises that lead to chemical reactions and particle ionizations.

In order to study the interaction of molecules with surfaces, it is mandatory to have a reliable description of the interaction energetics. The basic quantity reflecting this interaction is the potential energy surface (PES) that corresponds to a hyperplane in the multidimensional configuration space.
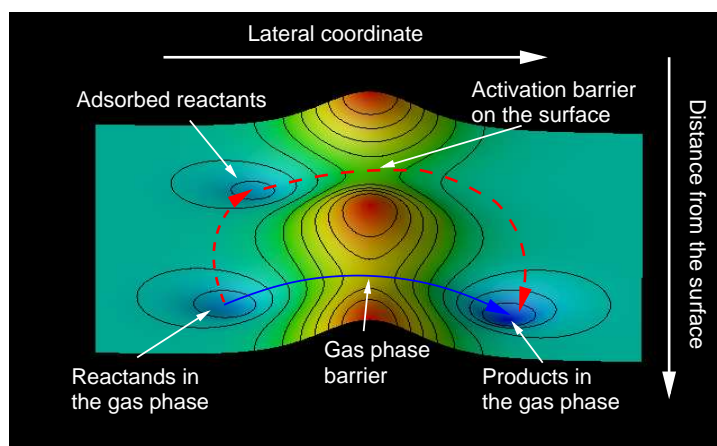
Figure 1: Schematic illustration of the role of a catalyst using a two-dimensional representation of the potential energy surface. A catalyst provides a detour in the multi-dimensional PES with lower activation barriers

Nowadays potential energy surfaces can be mapped out in great detail by first-principles electronic structure calculations, typically based on density functional theory. From the PES, quantities such as adsorption or binding energies, transition state configurations and energies or minimum energy paths can be derived.

Potential energy surface can also be used to illustrate processes at surfaces. An example is given in Fig. 1 explaining the way a catalyst works. The presence of a catalysts lowers the activation barrier for a particular chemical reaction, however, this involves a detour in the multi-dimensional PES on the path from the reactants to the products. In heterogeneous catalysis, this usually means that the reactants have to be adsorbed on the catalyst surface, where the activation barrier is much smaller than for example in the gas phase. Hence the reaction rate is enormously enhanced in the presence of a catalyst since the rate depends exponentially on the barrier height.

For a true understanding of processes on and at surfaces, however, the static information from total-energy calculations is often not sufficient. Furthermore, experiments do usually not yield direct information about the potential energy surface, but rather determine reaction probabilities or transfer rates. In order to calculate these quantities and allow for a genuine comparison between theory and experiment, dynamical or kinetic simulations are required. Unfortunately, processes such as chemical reactions at surfaces often consist of many elementary steps which are too complex to be studied as a whole. Therefore in surface science one tries to understand reaction mechanisms by breaking them up into simpler steps which are then studied under well-defined conditions [2].

In this chapter, I will briefly review the theoretical methods necessary to determine the dynamics of processes at surfaces. After presenting classical and quantum methods, scattering at surfaces will be addressed. A substantial fraction of the chapter will then be devoted to the discussion of atomic, molecular and dissociative adsorption. Finally, the system $O_2/Pt(111)$ will be discussed as an example, where scattering, molecular and dissociative adsorption can all occur.

2 Molecular Dynamics

In order to follow the temporal evolution of a dynamical system, the corresponding quantum or classical equations of motion have to be solved. They can be derived from the basic equations describing the interaction of atoms and molecules with each other, namely the non-relativistic Schrödinger equation on which most of chemistry and solid-state physics is based. It is of the general form

$$H\Psi(\{\mathbf{R},\mathbf{r}\})\rangle = E \ \Psi(\{\mathbf{R},\mathbf{r}\}) . \tag{1}$$

where the $\mathbf{R}$ are the ionic coordinates and $\mathbf{r}$ the electronic coordinates. It is well-known that a complete analytical solution of the Schrödinger equation taking into account both ionic and electronic degrees of freedom is not possible except for simple cases. One common approach is to assume that – because of the large mass difference between electrons and the nuclei – the electrons follow the motion of the nuclei adiabatically. This is the so-called Born-Oppenheimer approximation [3].

In practice, in the Born-Oppenheimer approximation the nuclear coordinates are fixed so that they enter the Schrödinger equation no longer as variable but just as parameters. Thus one obtains an electronic Schrödinger equation

$$H_{\mathrm{el}} \ (\{\mathbf{R}\}) \ \psi(\{\mathbf{r}\}) = E_{\mathrm{el}} \ (\{\mathbf{R}\}) \ |\psi(\{\mathbf{r}\}). \tag{2}$$

The many-electron ground state energy $E_{\mathrm{el}}(\{\mathbf{R}\})$ then defines the potential energy surface for the motion of the nuclei. For extended systems the most efficient approach to determine the many-electron ground state energy $E_{\mathrm{el}}(\{\mathbf{R}\})$ from first principles is density functional theory (DFT) [4] in combination with the supercell concept. Once the electronic ground state energy is obtained, it can be plugged into the Schrödinger equation for the nuclei,

$$\left(\sum_i \frac{-\hbar^2}{2M_i}\nabla^2_{\mathbf{R}_i} + E_{\mathrm{el}}(\{\mathbf{R}\})\right) \Phi(\{\mathbf{R}_m\}) = E_{\mathrm{nucl}} \ \Phi(\{\mathbf{R}\}), \tag{3}$$

where E_{nucl} is now the energy relevant for the dynamics of the nuclei. Alternatively, the potential energy surface can be used to solve the classical equations of motion,

$$M_i \ \frac{\partial^2}{\partial t^2}\mathbf{R}_i = -\frac{\partial}{\partial \mathbf{R}_i}E_{\mathrm{el}}(\{\mathbf{R}_m\}) \quad . \tag{4}$$

Instead of Newton's equation of motion, also Hamilton's equation of motion

$$\dot{q} = \frac{\partial H}{\partial p} \quad \dot{p} = -\frac{\partial H}{\partial q} \ . \tag{5}$$

can be solved.

The solution of the equations of motion can be obtained by standard numerical integration schemes like Runge–Kutta, Bulirsch–Stoer or predictor-corrector methods (see, e.g., [5]). Very often the rather simple Verlet algorithm [6, 7] is used which is easily derived from a Taylor expansion of the

trajectory.

$$\begin{aligned}
\mathbf{r}_i(t+h) &= \mathbf{r}_i(t) + h\left.\frac{d\mathbf{r}_i}{dt}\right|_{h=0} + \frac{h^2}{2}\left.\frac{d^2\mathbf{r}_i}{dt^2}\right|_{h=0} + \frac{h^3}{6}\left.\frac{d^3\mathbf{r}_i}{dt^3}\right|_{h=0} + \ldots \\
&= \mathbf{r}_i(t) + h\,\mathbf{v}_i(t) + \frac{h^2}{2}\frac{\mathbf{F}_i(t)}{m} + \frac{h^3}{6}\left.\frac{d^3\mathbf{r}_i}{dt^3}\right|_{h=0} + \ldots \quad (6)
\end{aligned}$$

Here we have introduced the velocity $\mathbf{v}_i = \dot{\mathbf{r}}_i$. Furthermore, we have used Newton's equation of motion to include the force $\mathbf{F}_i$ acting on the i-th particle. Analogously we can derive

$$\mathbf{r}_i(t-h) = \mathbf{r}_i(t) - h\,\mathbf{v}_i(t) + \frac{h^2}{2}\frac{\mathbf{F}_i(t)}{m} - \frac{h^3}{6}\left.\frac{d^3\mathbf{r}_i}{dt^3}\right|_{h=0} + \ldots \quad (7)$$

Adding (6) and (7) yields the Verlet algorithm [6]

$$\mathbf{r}_i(t+h) = 2\mathbf{r}_i(t) - \mathbf{r}_i(t-h) + h^2\frac{\mathbf{F}_i(t)}{m} + O(h^4) . \quad (8)$$

The accuracy of the numerical integration of the equation of motion can be checked by testing the energy conservation. In order to evaluate the kinetic energies, the velocities at time t are needed. Note that they do not explicitly appear in Eq. (8). They can be estimated by

$$\mathbf{v}_i(t) = \frac{\mathbf{r}_i(t+h) - \mathbf{r}_i(t-h)}{2h} . \quad (9)$$

However, the kinetic energy evaluated with Eq. (9) belongs to the time step prior to the one used for the positions (8) which enter the evaluation of the potential energy. This problem can be avoided in the so-called *velocity* Verlet algorithm [7]

$$\begin{aligned}
\mathbf{r}_i(t+h) &= \mathbf{r}_i(t) + h\,\mathbf{v}_i(t) + \frac{h^2}{2}\frac{\mathbf{F}_i(t)}{m} \\
\mathbf{v}_i(t+h) &= \mathbf{v}_i(t) + h\frac{\mathbf{F}_i(t+h) + \mathbf{F}_i(t)}{2m} , \quad (10)
\end{aligned}$$

which is mathematically equivalent to the Verlet algorithm.

In Fig. 2, various processes that can occur when atoms or molecules are impinging on a surface are illustrated. For all atoms that are heavier than hydrogen or helium, the quantum effects in the dynamics are often negligible [8]. Hence molecular dynamics simulations involving the solution of the classical equations of motion are an appropriate tool to determine the time evolution of most chemical systems. Even if hydrogen is contained in the system as is generally the case for organic molecules, still the results of classical dynamical calculations might be meaningful qualitatively or semi-quantitatively. However, for a real quantitative description, a quantum treatment is necessary. Furthermore, there are certain phenomena in the gas-surface interaction that can only be understood within a quantum framework, namely elastic scattering and diffraction.

There are two ways to determine quantum mechanical reaction probabilities: by solving the time-dependent or the time-independent Schrödinger equation. Both approaches are equivalent [9] and should give the same results. The answer to the question which method is more appropriate depends
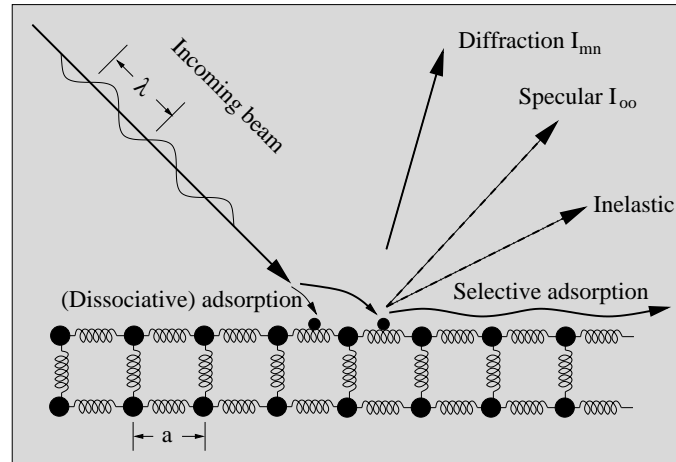
Figure 2: Illustration of the different processes that can occur when atoms or molecules are imping-ing on a surface. The substrate with lattice constant a is represented in a simple ball and spring picture.

on the particular problem. Time-independent implementations are usually more restrictive as far as the form of the potential is concerned, but often the choice of the method is a matter of training and personal taste.

In the time-dependent or wave-packet formulation, the solution of the time-dependent Schrödinger equation

$$i\hbar \frac{\partial}{\partial t} \Psi(\mathbf{R}, t) = H \Psi(\mathbf{R}, t) \tag{11}$$

can formally be written as

$$\Psi(\mathbf{R}, t) = e^{-iHt/\hbar} \Psi(\mathbf{R}, t = 0) , \tag{12}$$

if the potential is time-independent. The most common methods to represent the time-evolution operator $\exp(-iHt/\hbar)$ in the gas-surface dynamics community are the split-operator [10, 11] and the Chebychev [12] methods. In the split-operator method, the time-evolution operator for small time steps Δt is written as

$$e^{-iH\Delta t/\hbar} = e^{-iK\Delta t/2\hbar} e^{-iV\Delta t/\hbar} e^{-iK\Delta t/2\hbar} + O(\Delta t^3) , \tag{13}$$

where K is the kinetic energy operator and V the potential term. In an alternative approach, the Chebyshev method, the time-evolution operator is expanded as

$$e^{-iH\Delta t/\hbar} = \sum_{j=1}^{j_{\max}} a_j(\Delta t) T_j(\bar{H}) , \tag{14}$$

where the T_j are Chebyshev polynomials and $\bar{H}$ is the Hamiltonian rescaled to have eigenvalues in the range $(-1, 1)$. Both propagation schemes use the fact that the kinetic energy operator is diagonal in $\mathbf{k}$-space and the potential is diagonal in real-space. The wave function and the potential are represented on a numerical grid, and the switching between the $\mathbf{k}$-space and real-space representations is efficiently done by Fast Fourier Transformations (FFT) [5].

In the time-independent formulation, on the other hand, the wave function is usually expanded in a suitable basis set. This often requires to introduce the concept of reaction path coordinates. Starting from the time-independent Schrödinger equation

$$(H - E) \Psi = 0 \ , \tag{15}$$

one specific reaction path coordinate s is chosen. Then the kinetic energy operator in this coordinate is separated yielding

$$(\frac{-\hbar^2}{2\mu}\partial_s^2 + \tilde{H}E) \ \Psi = 0 \ . \tag{16}$$

Here $\tilde{H}$ is the original Hamiltonian except for the kinetic energy operator in the reaction path coordinate. Usually the use of curve-linear reaction path coordinates results in a more complicated expression for the kinetic energy operator involving cross terms, but for the sake of clarity this has been neglected in Eq. (16). In the coordinates perpendicular to the reaction path coordinate, the wave function is expanded in some suitable set of basis functions,

$$\Psi = \Psi(s, \dots) = \sum_n \ \psi_n(s) \ |n\rangle \ . \tag{17}$$

Here n is a multi-index, and the expansion coefficients $\psi_n(s)$ are assumed to be a function of the reaction path coordinate. This expansion of Ψ is inserted in the Schrödinger equation (16), and this equation is multiplied by $\langle m|$ which corresponds to performing a multi-dimensional integral. Since the basis functions $|n\rangle$ are assumed to be independent of s, this yields the so-called coupled-channel equations

$$\sum_n \left\{ (\frac{-\hbar^2}{2\mu}\partial_s^2 - E) \ \delta_{m,n} + \langle m|\tilde{H}|n\rangle \right\} \psi_n(s) = 0 \ . \tag{18}$$

Instead of a high-dimensional partial differential equation – the original time-independent Schrödinger equation (15) – there is now a set of coupled ordinary differential equation. Still a straightforward numerical integration of the coupled-channel equations leads to instabilities, except for in simple cases, due to exponentially increasing so-called closed channels. These problems can be avoided, for example by making the potential stepwise constant so that the wave function can be analytically propagated [13, 14]

3 Scattering at surfaces

In Fig. 2, possible collision processes in the scattering of atoms and molecules at surfaces are summarized. A monoenergetic beam of atoms or molecules characterized by the wave vector $\mathbf{K}_i = \mathbf{P}_i/\hbar$ where $\mathbf{P}_i$ is the initial momentum of the particles is impinging on a periodic surface with lattice constant a. Classically there will always be a certain energy transfer from the molecules to the substrate when the incoming particles hit the surface. Quantum mechanically, however, there will be a non-vanishing probability for elastic scattering, i.e. with no energy transfer to the substrate. This probability is given by the so-called Debye-Waller factor.

Furthermore, if the de Broglie wavelength $\lambda = 1/|\mathbf{K}_i|$ of the incident beam is of the order of the lattice spacing a, quantum effects in the momentum transfer parallel to the surface become

important. The periodicity of the substrate leads to the conservation of the quasi-momentum parallel to the surface which means that the component of the wave vector parallel to the surface can only be changed by a reciprocal lattice vector of the periodic surface:

$$\mathbf{K}_f^{\parallel} = \mathbf{K}_i^{\parallel} + \mathbf{G}_{mn} , \tag{19}$$

where $\mathbf{G}_{mn}$ is a reciprocal lattice vector of the periodic surface and $\mathbf{K}_i^{\parallel}$ and $\mathbf{K}_f^{\parallel}$ are the initial and final wave vectors parallel to the surface. As a consequence, diffraction results, i.e., there is only a discrete number of allowed scattering angles. The intensity of the elastic diffraction peak mn according to Eq. (19) is denoted by I_{mn}. The scattering peak I_{00} with $\mathbf{K}_f^{\parallel} = \mathbf{K}_i^{\parallel}$ is called the *specular peak*. It is important to note that the allowed scattering angles are a consequence of the surface geometry which means that from the diffraction pattern the periodicity and lattice constant of the surface can be derived, whereas the intensity of the different diffraction peaks depends on the particular molecule-surface system. Therefore the coherent scattering of atoms or molecules from surfaces can be used as a tool for probing surface structures which has first been realized in 1930 [15]. In particular helium atom scattering (HAS) experiments have been carried out to study the surface crystallography (see, e.g., [16, 17] and references therein).

The probability for elastic scattering, i.e. the Debye-Waller factor, vanishes rapidly with increasing mass of the impinging molecules. For heavier molecules, predominantly inelastic scattering occurs. The main source for the energy transfer between the impinging molecules and the substrate is the excitation and deexcitation of substrate phonons but also electron-hole pairs of the substrate may be involved. Since phonons also carry momentum, the conservation of quasi-momentum parallel to the surface is modified to

$$\mathbf{K}_f^{\parallel} = \mathbf{K}_i^{\parallel} + \mathbf{G}_{mn} + \sum_{\text{exch.phon.}} \pm\mathbf{Q} , \tag{20}$$

where $\mathbf{Q}$ is a two-dimensional phonon-momentum vector parallel to the surface. The plus-signs in the sum correspond to the excitation or emission of a phonon while the minus-signs represent the deexcitation or absorption of a phonon. The energy balance in phonon-inelastic scattering can be expressed as

$$\frac{\hbar^2 \mathbf{K}_f^2}{2M} = \frac{\hbar^2 \mathbf{K}_i^2}{2M} + \sum_{\text{exch.phon.}} \pm\hbar\omega_{\mathbf{Q},j} , \tag{21}$$

where $\hbar\omega_{\mathbf{Q},j}$ corresponds to the energy of the phonon with momentum $\mathbf{Q}$ and mode index j. From the change of the momentum and the energy in single-phonon scattering, the surface phonon spectrum can be derived which has been extensively done using helium atom scattering as a probe [16, 18]. The excitation of phonons usually leads to a reduced normal component of the kinetic energy of the back-scattered atoms or molecules. Thus the reflected beam is shifted in general to larger angles with respect to the surface normal compared to the angle of incidence. The resulting supraspecular scattering is indicated in Fig. 2 as the inelastic reflection event.

In addition to diffraction, often resonances in the intensity of the specular peak as a function of the angle of incidence are observed in the case of the scattering of weakly interacting particles at smooth surfaces, [19]. These so-called *selective adsorption resonances* are also indicated in Fig. 2. They occur when the scattered particle can make a transition into one of the discrete bound state

of the adsorption potential [20]. This is only possible if temporarily the motion of the particle is entirely parallel to the surface. The interference of different possible paths along the surface causes the resonance effects. Energy and momentum conservation yields the selective adsorption condition

$$\frac{\hbar^2 \mathbf{K}_i^2}{2M} \;=\; \frac{\hbar^2 (\mathbf{K}_i^{\parallel} + \mathbf{G}_{mn})^2}{2M} \;-\; |E_l| \;, \tag{22}$$

where E_l is a bound level of the adsorption potential. From the scattering resonances, bound state energies can be obtained using Eq. (22) without any detailed knowledge about the scattering process.

Since molecules, in contrast to atoms, have also internal degrees of freedoms, namely rotations and vibrations, additional peaks may appear in the diffraction pattern of molecules. They are due to the fact that these rotations and vibrations can be excited and de-excited during the collision process. The total energy balance in the molecular scattering is therefore more complex:

$$\frac{\hbar^2 \mathbf{K}_f^2}{2M} = \frac{\hbar^2 \mathbf{K}_i^2}{2M} + \Delta E_{\text{rot}} + \Delta E_{\text{vib}} \;+\; \sum_{\text{exch.phon.}} \pm \hbar \omega_{\mathbf{Q},j} \;. \tag{23}$$

Since the time-scale of the molecular vibrations is usually much shorter than the scattering time or the rotational period and therefore the associated excitation energies are much larger, the excitation of molecular vibrations in molecule-surface scattering is usually negligible, in contrast to the phonon excitation. Molecular rotations, on the other hand, can be excited rather efficiently in the scattering at highly corrugated and anisotropic surfaces. This leads to additional peaks in the diffraction spectrum, the *rotationally inelastic diffraction* peaks.

Experimentally, rotationally inelastic diffraction of hydrogen molecules has been first observed in the scattering at inert ionic solids such as MgO [21] or NaF [22]. At metal surfaces with a high barrier for dissociative adsorption, the molecules are scattered at the tails of the metal electron density which are usually rather smooth. Hence relatively weak diffraction and hardly any rotationally inelastic diffraction has been observed for, e.g., the scattering of H_2 from Cu(001) [23, 24]. This is different for the case of HD scattering, where the displacement of the center of mass from the center of the charge distribution leads to a strong rotational anisotropy [25].

At reactive surfaces where non-activated adsorption is possible, the scattering occurs rather close to the surface where the potential energy surface is already strongly corrugated and anisotropic. For such systems, intensive rotationally inelastic peaks in the diffraction pattern have been predicted theoretically in six-dimensional quantum dynamical calculations [26] for the scattering of H_2/Pd(100) where non-activated together with activated pathways to dissociative adsorption exist. One typical calculated angular distribution of H_2 molecules scattered at Pd(100) is shown in Fig. 3 [26]. The total initial kinetic energy is $E_i = 76$ meV. The incident parallel momentum equals $2\hbar G$ along the $\langle 0\bar{1}1 \rangle$ direction which corresponds to an incident angle of $\theta_i = 32°$. The molecules are initially in the rotational ground state $j_i = 0$. Figure 3a shows the so-called in-plane scattering distribution, i.e. the diffraction peaks in the plane spanned by the wave vector of the incident beam and the surface normal. The label (m, n) denotes the parallel momentum transfer $\Delta \mathbf{G}_{\parallel} = (mG, nG)$. The specular peak is the most pronounced one, but the first order diffraction peak (10) is only a factor of four smaller. Note that in a typical helium atom scattering experiment the off-specular peaks are about two orders smaller than the specular peak [16]. This is due to
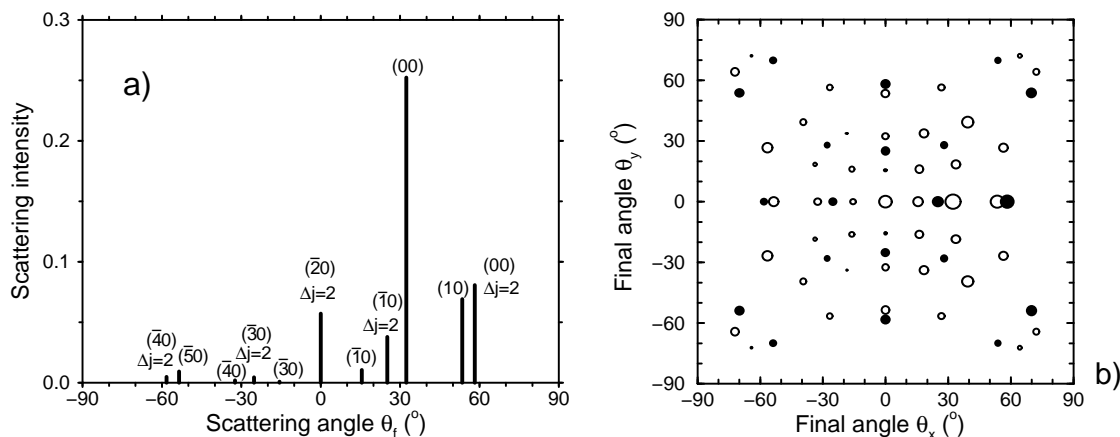
Figure 3: Diffraction spectrum of H_2 scattered at Pd(100) for a kinetic energy of 76 meV at an incidence angle of $32°$ along the [10] direction of the square surface lattice, obtained by six-dimensional quantum coupled channel calculations. a) In-plane diffraction spectrum where all peaks have been labeled according to the transition. b) In-plane and out-of-plane diffraction peaks. The open and filled circles correspond to the rotationally elastic and rotationally inelastic scattering, respectively, with he radius of the circles being proportional to the logarithm of the scattering intensity (after [26]).

the fact that the chemically inert helium atoms are scattered at the smooth tails of the surface electron distribution.

The peaks labeled with $\Delta j = 2$ in Fig. 3a correspond to rotationally inelastic diffraction involving the rotational excitation $j = 0 \rightarrow 2$ summed up over all final azimuthal quantum numbers m_j. Except for the specular peak, the intensities of the rotationally inelastic diffraction peaks are even larger than the corresponding rotationally elastic diffraction peaks with the same momentum transfer (m, n). Note that because of the particular conditions with the incident parallel momentum corresponding to the reciprocal lattice vector $\mathbf{G}_{\parallel} = (2G, 0)$, the rotationally elastic and inelastic $(\bar{2}0)$ diffraction peaks fall upon each other.

The full diffraction pattern including also the so-called out-of-plane scattering peaks is shown in Fig. 3b. The open circles represent the rotationally elastic, the filled circles the rotationally inelastic diffraction peaks. The radii of the circles are proportional to the logarithm of the scattering intensity. It is obvious that there is a significant fraction of out-of-plane scattering with the sum of all out-of-plane scattering intensities approximately equal to the sum of all in-plane scattering intensities. Interestingly, some diffraction peaks with a large parallel momentum transfer still show substantial intensities. This phenomenon is well known from helium atom scattering and has been discussed within the concept of so-called rainbow scattering [27].

Experimentally, it is not so easy to measure diffraction patterns at reactive surfaces since during the experiment, a significant fraction of the impinging molecules remains on the surface which destroys the ideal periodicity of the surface and therefore also suppress the occurrence of diffraction patterns.

Thus the surface has to be kept clean which is achieved by relatively high surface temperatures so that adsorbates quickly desorb again. High surface temperatures, on the other hand, also smear out the diffraction pattern. Still rotationally inelastic peaks in addition to rotationally elastic peaks have been clearly identified in the diffraction pattern of D_2/Ni(110) [28] and D_2/Rh(110) [29].

At reactive surfaces, the particles can off course also adsorb. As it is indicated in Fig. 2, molecules can adsorb both molecularly which means intact or dissociatively. In the case of the atomic or molecular adsorption, the particles can only remain trapped at the surface if their initial kinetic is transfered to the surface and dissipated. For light projectiles, the quantum nature of the substrate phonons becomes important in the energy transfer process. These topics will be discussed in the next section.

4 Atomic and molecular adsorption

The sticking or adsorption probability is defined as the fraction of atoms or molecules impinging on a surface that are not scattered back, i.e. that remain on the surface. It is important to note that in the case of atomic or molecular adsorption when the molecule stays intact, the particles can only remain on the surface if they transfer their energy to the substrate. This is similar to gas-phase reactions where a bond between two reactants can only be formed in a three-body collision where a third reaction partner has to carry away the energy gained by the reaction unless there are other dissipation channels such as radiation.

At a surface, there are two main channels for energy dissipation namely phonon and electron-hole pair excitations. Here we focus on the energy transfer to phonons since they usually represent the main channel for dissipation [30]. For the explicit evaluation of sticking probabilities, $P_E(\epsilon)$ is defined as the probability that an incoming particle with kinetic energy E transfers the energy ϵ to the surface. Only if the particle transfers more than its initial energy to substrate excitations, it can remain at the surface. Hence the sticking probability can be expressed as

$$S(E) = \int_E^\infty P_E(\epsilon) \, d\epsilon. \tag{24}$$

In order to discuss the essentials of atomic and molecular adsorption due to the energy transfer to phonons, we will use the rather simple *hard-cube model* (HCM) [31, 32]. In this model that is schematically illustrated in Fig. 4a, the impact of the atom on the surface is treated as a binary elastic collision between a gas phase atom (mass m) and a substrate atom (mass M_c) which is moving freely with a velocity distribution $P_c(v_c)$. Because of the adsorption well of depth E_{ad}, the particle is accelerated and impinges on the hard cube with a velocity

$$v_{\text{well}} = -\sqrt{v_{\text{g}}^2 + \frac{2E_{\text{ad}}}{m}} \; . \tag{25}$$

Due to the simplicity of the hard cube model, it can be solved analytically [32]. Assuming a weighted Maxwellian velocity distribution for v_c, the trapping probability becomes

$$S_{\text{trap}}(v_{\text{g}}) = \frac{1}{2} + \frac{1}{2} \, \text{erf}(\alpha v_{\text{lim}}) + \frac{\exp\left\{-\alpha^2 v_{\text{lim}}^2\right\}}{2\sqrt{\pi}\alpha v_{\text{well}}} \; , \tag{26}$$
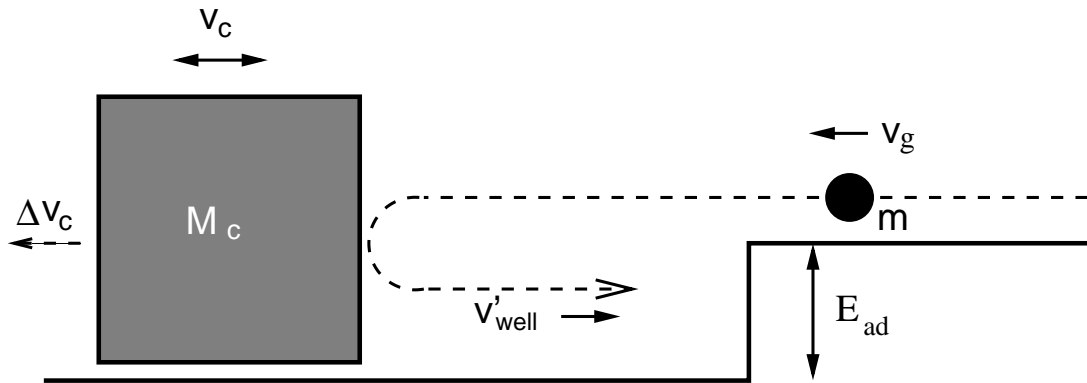
Figure 4: Hard cube model. a) Schematic illustration of the model. An atom or molecule with mass m is impinging in an attractive potential with well depth E_{ad} on a surface modeled by a cube of effective mass M_c. The surface cube is moving with a velocity v_c given by a Maxwellian distribution. b) Trapping probability as a function of the kinetic energy evaluated according to the hard cube model Eq. (26) for different adsorption energies E_{ad}, mass ratios $\mu = m/M_c$ and surface temperatures T_s.

where $\alpha = \sqrt{M_c/2k_{\mathrm{B}}T_{\mathrm{s}}}$, v_{lim} is given by

$$ v_{\mathrm{lim}} = \frac{\mu+1}{2}\sqrt{\frac{2E_{\mathrm{ad}}}{m}} - \frac{\mu-1}{2}v_{\mathrm{well}} \; , \tag{27} $$

and μ is the mass ratio $\mu = m/M$.

Typical sticking curves obtained with the hard cube model are shown in Fig. 4b. All curves show the same behavior, namely a monotonic decrease of the sticking probability as a function of the kinetic energy. This dependence is a consequence of the fact that the energy transfer to the surface becomes less efficient at higher kinetic energies. Although more energy is transfered to the surface at higher kinetic energies, the fraction of particles that loose more energy than their initial kinetic energy becomes smaller.

The examples shown in Fig. 4b have been chosen in order to illustrate further general trends in atomic adsorption. If the mass ratio between the impinging molecules and the substrate atoms increases, i.e. if heavier atoms are hitting the surface, more energy is transfered to the surface so that the trapping probability increases. If the adsorption well becomes deeper, the impinging molecules become faster and loose more energy upon impact which also increases the trapping probability. For an adsorption well of 0.6 eV, the effect of changing the surface temperature is shown. A higher surface temperature T_s leads to a broader velocity distribution which results in an averaging over a wider range of kinetic energies. This causes a decrease for negative curvature of the sticking curve, i.e. at high sticking probabilities, and an increase for positive curvature, i.e. at low sticking probabilities.

Adsorption well depths have often been estimated by fitting measured trapping probabilities to curves derived from the hard cube model, also for molecular adsorption (see, e.g., [32, 33]). In the simple hard cube model the surface is flat and structureless which means that in any scattering and adsorption process the incident parallel momentum is conserved. For the sticking probability
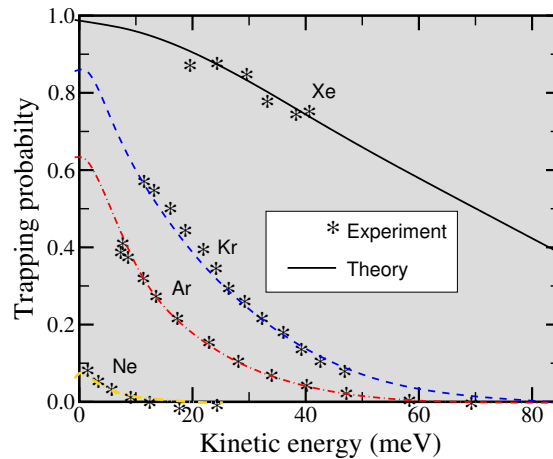
Figure 5: Sticking probability of rare gas atoms on $\mathrm{Ru}(0001)$ at a surface temperature of $T_s = 6.5\,\mathrm{K}$. Stars (*): experiment; lines: theoretical results obtained with the forced oscillator model (after [34], not all measured data points are included)

this leads to the *normal energy scaling*, i.e., the sticking probability is a function of the normal component $E_i \cos^2 \theta_i$ of the incident energy alone, where θ_i is the angle of incidence. Real surfaces, however, are not structureless as far as the interaction of atoms and molecules is concerned since adsorption corresponds to the making of a chemical bond which strongly depends on the local environment. This leads to *corrugation* in the potential energy surface, i.e., the potential depends on the lateral position of the interacting particle on the surface. Trapping probabilities often scale as $E_i \cos^n \theta_i$ with $n < 2$. An exponent of $n = 0$ corresponds to *total energy scaling* which is usually associated with a highly corrugated potential energy surface.

A further prediction of the hard cube model is that the sticking probability in the limit $E \to 0$ and $T_s \to 0$ always becomes unity no matter how small the adsorption well, no matter how small the mass ratio between the impinging atom and the substrate oscillator, if there is no barrier before the adsorption well. This is due to the energy transfer to the surface which in the limit of zero energy does not allow the particle to return into the gas-phase.

Experiments indeed show that for many adsorption systems all impinging particles become trapped at low kinetic energies, for example in the case of Xe impinging on $\mathrm{Ru}(0001)$ [35, 34] which is shown in Fig. 5. However, for the lighter rare gases Kr, Ar and in particular Ne the trapping probability extrapolated to $E \to 0$ is clearly below one. This behavior can not be reproduced using classical mechanics [35], instead it can only be understood if the quantum nature of the substrate phonon system is taken into account leading to a non-zero probability for elastic scattering at the surface. A classical treatment of the solid is only appropriate if the energy transfer to the surface is large compared to the Debye energy of the solid [36].

The essential physics can be captured by just considering an atomic projectile interacting via linear coupling with a single quantum surface oscillator in the so-called *trajectory approximation*. In this model, the classical motion of the incoming particle is assumed not to be perturbed by the coupling to the surface oscillator. The classical trajectory then introduces a time-dependent force

in the Hamiltonian of the oscillator

$$H_{\text{osc}} = \hbar\omega \, (a^+ a + \frac{1}{2}) + \lambda(t) \, (a^+ + a) \, , \tag{28}$$

In this *forced oscillator model* [37, 38, 39], the mean number of excited phonon $\bar{n}$ is given basically by the square of the Fourier transform of the coupling $\lambda(t)$,

$$\bar{n} = \left| \frac{1}{\hbar} \int_{-\infty}^{\infty} e^{i\omega t'} \, \lambda(t')dt' \right|^2 . \tag{29}$$

The number $\bar{n}$ also enters the expression of probability P_{ji} for a transition from an initial oscillator state i to the final state j [37]:

$$P_{ji} = \frac{i!}{j!} \, e^{-\bar{n}} \, \bar{n}^{j-i} \, [L_j^{j-i}(\bar{n})]^2 \, , \quad j \geq i \, . \tag{30}$$

Here L_j^{j-i} is an associated Laguerre polynomial [40]. For an excitation P_{j0} from the ground state one just obtains a Poisson distribution. The probabilities (30) yield the energy distribution of excited phonons and hence also the energy transfer from the impinging particle to the surface which that they correspond to the probability $P_E(\epsilon)$ entering the expression (24) for the sticking probability.

This forced oscillator model has been applied to evaluate the sticking probabilities of rare gas atoms on a Ru(001) surface at a temperature of $T_s = 6.5\,\text{K}$ [34]. Using the potential well depth, the potential range, the mass of the surface oscillator and the surface Debye temperature as parameters, this simple model was able reproduce the measured data quite well (see Fig. 5). In particular for the a light rare gas such as Ne impinging on a metal surface, the quantum effects in the surface recoil are quite substantial.

At even lower kinetic energies than reached in the experiments [34] shown in Fig. 5, the quantum nature of the impinging particles cannot be neglected any longer. Hence the trajectory approximation cannot be applied any more. In fact, in the limit $E \to 0$ the de Broglie wavelength of the incoming particle tends to infinity. In the case of a short-range attractive potential this means that the amplitude of the particle's wave function vanishes in the attractive region [36, 41]. Thus there is no coupling and consequently no energy transfer between the particle and the substrate vibrations. Therefore the quantum mechanical sticking probability also vanishes for $E \to 0$. However, in order to see this effect extremely small kinetic energies corresponding to a temperature below $0.1\,\text{K}$ are required [36]. Nevertheless, this quantum phenomenon in the sticking at surfaces has been verified experimentally for the adsorption of atomic hydrogen on thick liquid ^{4}He films [42].

5   Dissociative adsorption

In the case of dissociative adsorption there is another channel for energy transfer, namely the conversion of the kinetic and internal energy of the molecule into translational energy of the atomic fragments on the surface relative to each other. This bond-breaking process which is illustrated in
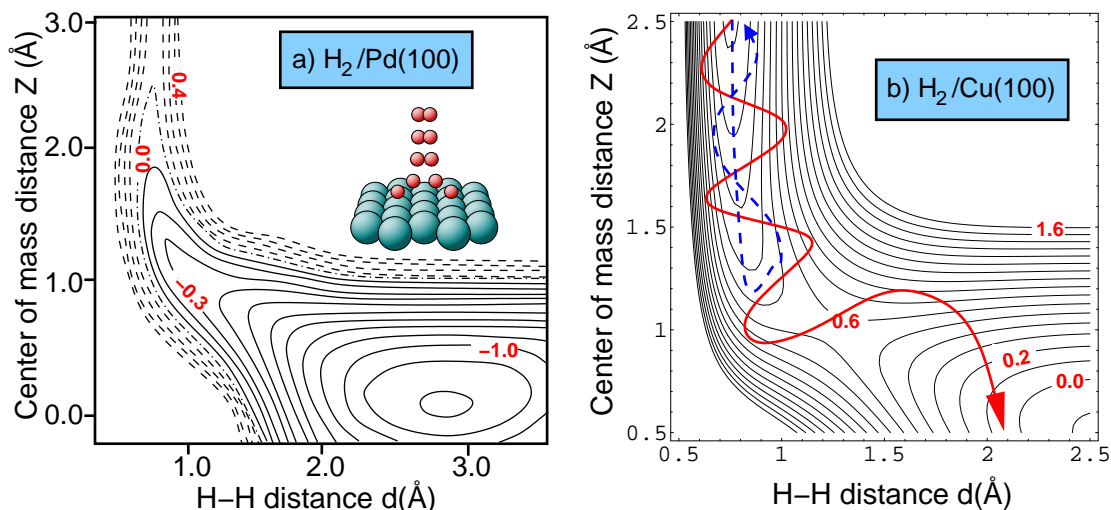
Figure 6: Contour plots of the potential energy surface along two-dimensional cuts through the six-dimensional coordinate space of H_2 in front of (100) metal surfaces determined by DFT-GGA calculations for H_2 molecules above the bridge site. The contour spacing is 0.1 eV per H_2 molecule. (**a**) H_2/Pd(100) (after [43]), (**b**) H_2/Cu(100) [44]. The inset is a) illustrates the process of dissociative adsorption while in b) two typical trajectories showing the effect of initial vibrations are included.

the inset of Fig. 6 represents the fundamental difference to atomic or molecular adsorption. As far as the complete adsorption process is concerned, it is true that eventually the atomic fragments will also dissipate their kinetic energy and come to rest at the surface. However, in the case of light molecules, in particular molecular hydrogen, dissociating on metal surfaces the energy transfer to the substrate is very small because of the large mass mismatch. Hence the probability for dissociative adsorption is almost entirely given by the initial dissociation probability upon the impact on the surface since the fragments do in general not directly recombine and desorb again. Therefore the dissociative adsorption process can be described within low-dimensional potential energy surfaces neglecting the surface degrees of freedom. This also requires that there is no substantial surface rearrangement upon adsorption, but this is usually the case in the dissociative adsorption on close-packed metal surfaces.

The dynamics of the interaction of hydrogen with metal surfaces has been well-studied, both experimentally [45] and theoretically [2, 46, 47, 48]. In Fig. 6, two cuts through the six-dimensional potential energy surface derived from DFT calculations for two benchmark systems are plotted, for H_2/Pd(100) where non-activated dissociation is possible [43]) and for the activated system H_2/Cu(100) [44]. The cuts including the respective minimum energy paths to dissociative adsorption correspond to so-called elbow plots which show the potential energy as a function of the H_2 center of mass distance from the surface and the H-H distance.

In order to quantitatively evaluate the adsorption probability of hydrogen, the full six-dimensional PES has to be known. Furthermore, the dynamics of hydrogen require a quantum treatment because of its light mass. Because of the high computational effort associated with quantum methods,
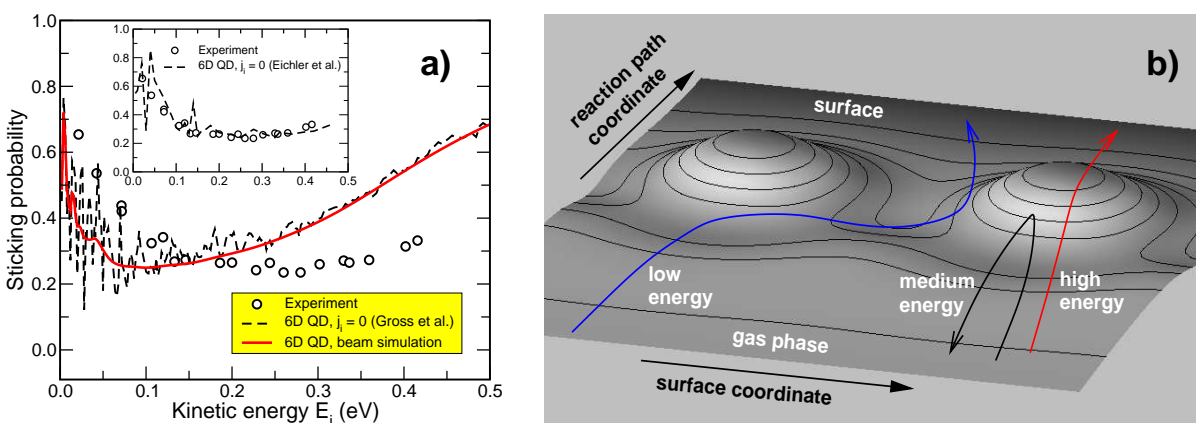
Figure 7: Dissociative adsorption of H_2/Pd(100). a) Sticking probability of H_2/Pd(100) as a function of the initial kinetic energy. Circles: experiment [51], dashed and solid line: theory according to H_2 initially in the ground state and with a thermal distribution appropriate for a molecular beam [49]. The inset shows the theoretical results using an improved *ab initio* potential energy surface [52]. b) Illustration of the steering effect.

for a long time the theoretical treatment was limited to studies within a reduced dimensionality. Only recently the first quantum studies were performed in which the full dimensionality of the hydrogen molecule was taken into account [49, 50].

The corresponding dissociative adsorption probability of H_2/Pd(100) is shown in Fig. 7a. Experiment [51] and theory [49, 52] agree well, as far as the qualitative trend of the adsorption probability as a function of the kinetic energy is concerned. First there is an initial decrease, and after a minimum the sticking probability rises again. The initial decrease of the sticking probability is typical for H_2 adsorption at transition metal surfaces [51, 53, 45, 54, 55]. Originally, such an initial decrease was associated with the existence of a molecular adsorption precursor state through which the dissociation was assumed to proceed. However, nowadays it is well established that this behavior in the dissociation of H_2 on reactive metal surfaces is caused by dynamical effects, namely *steering* [56, 49, 57] and *dynamical trapping* [58, 59, 60].

The steering effect is illustrated in Fig. 7b where typical trajectories are plotted as a function of a lateral coordinate and a reaction path coordinate which connects the molecule in the gas phase with the dissociated molecule on the surface. It is important to note that in these systems the PES shows purely attractive paths towards dissociative adsorption, but the majority of reaction paths for different molecular orientations and impact points exhibits energetic barriers hindering the dissociation. Still, at low kinetic energies most impinging molecules are steered towards the attractive dissociation channel leading to a high adsorption probability. In addition, the corrugation and anisotropy leads to a conversion of the kinetic energy of the impinging molecule into internal molecular degrees of freedom such as rotation and vibration and into lateral motion along the surface. This energy is then not available for a direct escape from the adsorption well so that the molecules become *dynamically trapped*. Both mechanisms that are only operative a low kinetic energies result large adsorption probabilities, and their suppression for higher kinetic energies leads to the decrease of the sticking probability. At even higher energies, the molecules can directly cross
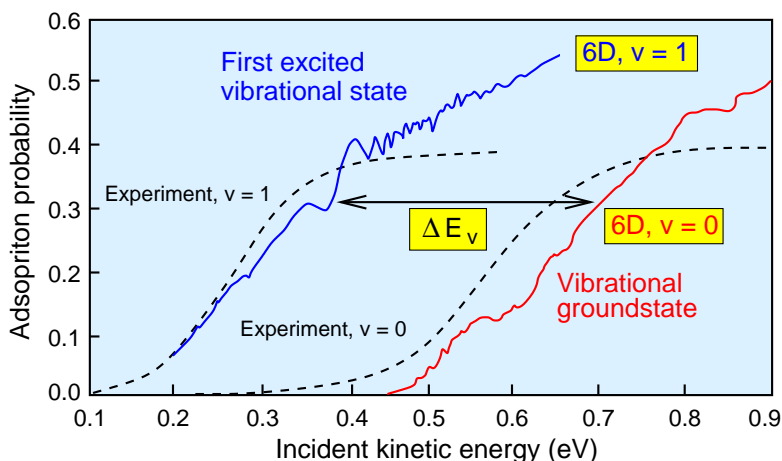
Figure 8: Dissociative adsorption probability of H_2 on Cu(100) as a function of the incident kinetic energy determined by six-dimensional quantum wave-packet calculations for molecules initially in the vibrational ground state and first excited state, respectively [61]. The calculations are compared to experimental results derived from an analysis of adsorption and desorption experiments [62].

the dissociation barriers causing again an increase in the adsorption probability.

As far as the activated adsorption is concerned, the interaction of hydrogen with copper surfaces has served as a model system [46, 47, 63, 64, 50, 65, 66]. It was also the first system for which high-dimensional potential energy surface were mapped out by DFT methods [67, 68, 69]. Figure 8 shows the calculated sticking probabilities for molecules either in the vibrational ground state or in the first excited state, respectively, based on an six-dimensional wave-packet calculations on an *ab initio* PES [50, 61]. The theoretical results are rather close to the experimental data which were derived from an analysis of both adsorption and desorption experiments [62] by using the following analytical form of the vibrationally resolved sticking probability as a function of the kinetic energy:

$$S_v(E) = \frac{A}{2}\left\{1 + \tanh\left(\frac{E - E_0(v)}{W(v)}\right)\right\} \tag{31}$$

The agreement between theory and experiment in Fig. 8 is very satisfactory except for the high-energy behavior. However, the experimental data of H_2 in Fig. 8 for kinetic energies above 0.5 eV were derived from thermal desorption experiments. As far the saturation value of the experimental sticking probability is concerned, there is a large uncertainty since the high energy contributions in desorption are exponentially suppressed through the Boltzmann factor.

The sticking probability of H_2/Cu(100) shows a typical activated behavior with an onset at approximately 0.5 eV for H_2 for molecules initially in the vibrational ground state. This onset is given by the minimum energy barrier including zero-point effects which arise from the quantization of the molecular levels due to the localization of the wave function at the minimum barrier position. The slope of the sticking probability is directly related to the distribution of the barrier heights for dissociative adsorption in the multidimensional potential energy surface [64]. Thus sticking can be understood in terms of the region of the surface that classically is available to dissociation. This so-called *hole model* [70] is valid at high kinetic energies when the incoming particles are not

significantly redirected by the shape of the potential energy surface.

As Fig. 8 demonstrates, for initially vibrationally excited molecules the sticking probability is significantly enhanced in the system H_2/Cu. Using the so-called *vibrational efficacy*,

$$\chi = \frac{\Delta E_v}{\hbar \omega_{\text{vib}}} \ , \tag{32}$$

where ΔE_v is the energetic shift between the sticking curves for molecules in the vibrationally ground and first-excited state, the vibrationally enhanced dissociation can be quantified. The shift ΔE_v is approximately $0.3\,\text{eV}$, as indicated in Fig. 8. Consequently, with the vibrational frequency of H_2, $\hbar\omega_{\text{vib}} = 0.516\,\text{eV}$, the vibrational efficacy becomes $\chi \approx 0.6$ which is often interpreted to mean that 60% of the vibrational energy is used to overcome the barrier for dissociative adsorption.

Vibrationally enhanced dissociation has been known for years in gas phase dynamics [71]. The basic mechanism can be discussed within a two-dimensional elbow plot as shown in Fig. 6b. The system H_2/Cu(100) exhibits a barrier which is located after the curved region of the minimum energy path which is called a *late barrier*. For such a topology of the PES, initial vibrations can be very helpful, as is illustrated with two typical trajectories in Fig. 6b. Initially non-vibrating molecules with a kinetic energy less than the barrier height are reflected at the adsorption barrier (dashed line). However, if the molecule is already initially vibrating, i.e., if it is oscillating back and forth in the *d*-direction, then the vibrational energy can be very efficiently used "to make it around the curve" and enter the dissociation channel. In addition, there are vibrationally adiabatic effects associated with the lowering of the vibrational frequency perpendicular to the reaction path which also contribute to the vibrationally enhanced dissociation [72].

In addition to the vibrational state, also the rotational state can have a significant influence on the dissociative adsorption probability. Usually additional rotational motion suppresses the adsorption probability because the molecule will rotate out of a favorable orientation for dissociation during the adsorption process [8]. Invoking the principle of microscopic reversibility of detailed balance, this leads to the so-called *rotational cooling* in desorption, i.e., the mean rotational energy is below the value expected for thermal equilibrium. Conversely, the vibrationally enhanced dissociation corresponds to *vibrational heating* in desorption.

6   The full concert: molecular and dissociative adsorption and scattering

In the examples discussed so far, we focused either on the energy transfer in atomic and molecular adsorption or on the bond-breaking process in dissociative adsorption. However, there are molecule-surface systems in which all these processes can occur at the same time. One example is the interaction of O_2/Pt(111). This is a well-studied system motivated by the fact that the adsorption of oxygen on platinum represents one of the fundamental microscopic reaction steps occuring in the car-exhaust catalyst. On Pt(111), there exist both physisorbed and chemisorbed molecular oxygen species [73, 74] as well as dissociatively adsorbed oxygen. The chemisorbed species have also been

identified in total-energy calculations [75, 76] using density functional theory (DFT) within the generalized gradient approximation (GGA) [77].

According to molecular beam experiments [78, 79], the sticking probability of O_2/Pt(111) first exhibits a strong decrease, and then after passing a minimum at approximately 0.15 eV the sticking probability levels off at a value of about 0.3 [78, 79]. Surprisingly, in molecular beam experiments it was also found that oxygen molecules do not dissociate at cold Pt surfaces below 100 K [33, 80, 79], even at kinetic energies above 1 eV which are much greater than the dissociation barrier.

The theoretical description of the adsorption dynamics of O_2/Pt(111) represents a significant challenge. On the one hand, a realistic PES is needed that reliably describes both the molecular as well as the dissociative adsorption channels. On the other hand, molecular trapping processes can only be reproduced if the energy dissipation to the platinum substrate is properly taken into account, as discussed in sect. 4. Direct *ab initio* molecular dynamics simulations represent a scheme that meets these requirements, but it is computationally still very expensive [2, 81]. Using empirical classical potentials, almost arbitrarily many trajectories can be computed, however, there are no reliable interaction potentials available treating reactions on the surface and the surface recoil upon impact on an equal footing.

As an intermediate method, tight-binding molecular dynamics simulations have been performed [82, 83] with the parameters of the tight-binding Hamiltonian derived from *ab initio* calculations [84, 75, 76]. In tight-binding, the exact many-body Hamiltonian is replaced by parameterized Hamiltonian matrix elements of the effective one-particle Hamiltonian in an atomic-like basis set. The atomic-like basis functions are usually not considered explicitly, but the matrix elements are assumed to have the same symmetry properties as matrix elements between atomic states. The evaluation of the tight-binding Hamiltonian still requires the diagonalization of a matrix, but it is about three orders of magnitude faster than corresponding *ab initio* calculations.

A comparison between the calculated [83] and the measured [78, 79] sticking probabilities is shown in Fig. 9a. It is obvious that the experimental data are qualitatively and even semi-quantitatively reproduced by the *ab initio* based tight-binding molecular dynamics calculations. It is important to note that also the experimental finding that O_2 does not directly dissociate upon adsorption is confirmed by the calculations.

There is a simple explanation for this result in terms of the topology of the elbow plots (see Fig. 9b). Dissociation corresponds to an event in which the molecules enter the exit channel towards the lower right corner of the figures. To enter this channel directly from the gas phase through the molecular adsorption state requires a sharp turn of the trajectories. In Fig. 9b, a trajectory of an O_2 molecule directly aimed at the molecular precursor state is included. Its kinetic energy of 0.6 eV is much higher than the dissociation barrier (~ 0.2 eV [76]); still it does not dissociate. It becomes accelerated by the attractive potential, hits the repulsive wall of the potential and is scattered back. This shows that direct dissociation of O_2/Pt(111) is not impossible, but it is very unlikely. Thus it follows that because of this steric hindrance, dissociation of O_2 on Pt(111) is a two-step process. First the molecule becomes trapped and accommodated in the molecular chemisorption state, and only subsequently it dissociates at sufficiently high surface temperatures due to thermal fluctuations which will make the O_2 molecules enter the dissociation channel.
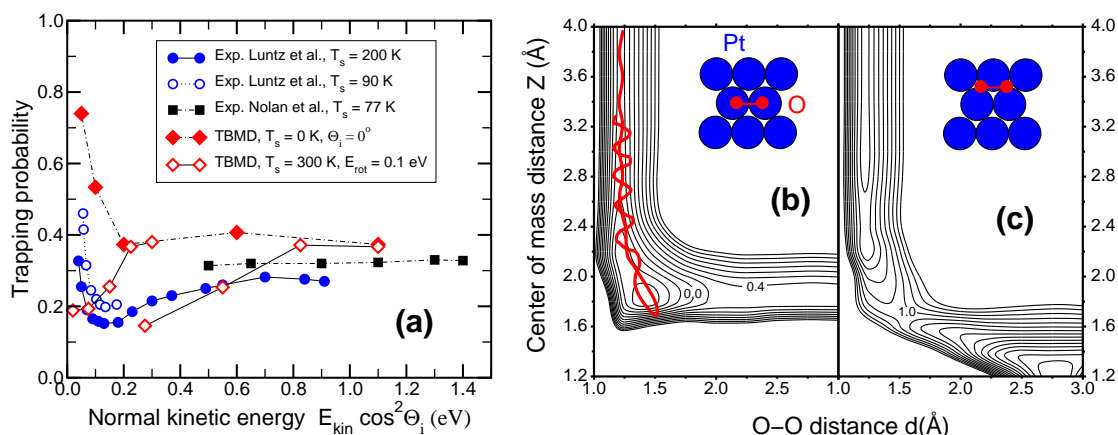
Figure 9: O_2 adsorption on Pt(111). a) Trapping probability of O_2/Pt(111) as a function of the normal component of the kinetic energy. Results of molecular beam experiments for surface temperatures of 90 K and 200 K (Luntz *et al.* [78]) and 77 K (Nolan *et al.* [79]) are compared to tight-binding molecular dynamics simulations for the surface initially at rest ($T_s = 0$ K). b and c) Elbow plots of the PES of the dissociation of O_2/Pt(111) determined by the *ab initio* derived tight-binding Hamiltonian [76, 83]. The configurations of the remaining O_2 degrees of freedom are illustrated in the insets. The contour spacing is 0.2 eV per O_2 molecule. In (b) a trajectory of an O_2 molecule with an initial kinetic energy of 0.6 eV scattered at Pt(111) is also plotted.

The molecular dynamics simulations also showed that contrary to common belief [33, 79] the strong initial decrease of the sticking probability is not caused by the trapping into a shallow physisorption state. Instead, the high sticking probability at low kinetic energies is again caused by the steering effect which becomes quickly suppressed for higher kinetic energies. Thus it is not the energy transfer *per se* that determines the sticking probability at low kinetic energies but rather the probability to enter the molecular chemisorption state. All molecules that find their way to the molecular chemisorption state at low kinetic energies do in fact remain trapped.

The magnitude of the steering effect is a consequence of the strong corrugation and anisotropy of the PES of O_2/Pt(111). The significant corrugation is illustrated in Figs. 9b and c. The lateral position of the O_2 center of mass is only shifted by about 1 Å between the two cuts. Nevertheless, there is no longer any chemisorption well present but rather a large barrier of about 1 eV towards dissociative adsorption which becomes even larger for the molecule directly at the on-top site. In fact, the majority of adsorption pathways are hindered by barriers; direct non-activated access to the adsorption states is possible for only a small fraction of initial conditions.

The strong corrugation and anisotropy of the PES has further consequences. First of all it leads to a high probability of dynamical trapping due to the conversion of the initial kinetic energy into internal molecular degrees of freedom which for this particular system is almost independent from the kinetic energy. This causes the leveling off of the trapping probability at higher kinetic energies. Furthermore, in Fig 9a the results of calculations for non-normal incidence are shown for two different total kinetic energies, $E_i = 0.3$ eV and 1.1 eV. Additional parallel momentum strongly suppresses the sticking probability, in agreement with the experiment [78]. It is obvious
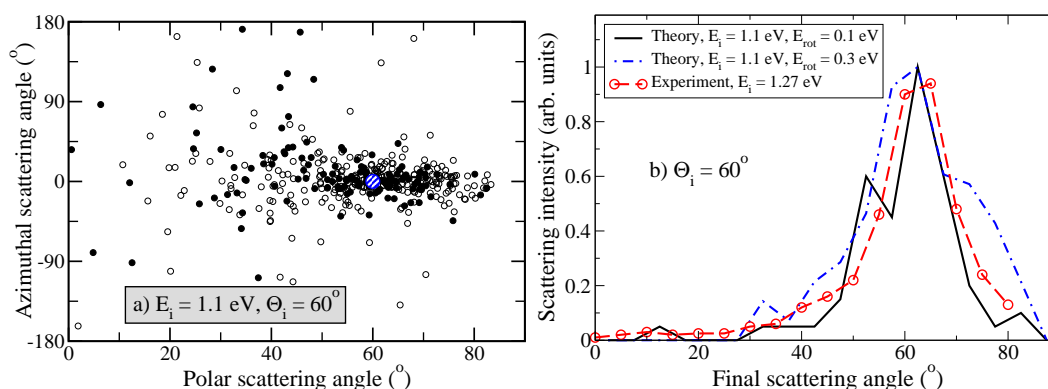
Figure 10: Angular distribution of O_2 scattered from Pt(111) with an angle of incidence of 60°. a) Calculated angular distribution (surface temperature $T_s = 300$ K) for an initial rotational energy of 0.1 eV (filled circles) and 0.3 eV (open circles). b) Comparison of the measured and the calculated angular distribution in in-plane scattering for an angle of incidence of 60°. The initial kinetic energy in the experiment was 1.27 eV [85] while the TBMD simulations have been performed for an initial energy of 1.1 eV. Theoretical results are shown for both an initial rotational energy of 0.1 eV and 0.3 eV.

that the trapping of O_2/Pt(111) does not obey normal energy scaling, i.e., it is not a function of the normal kinetic energy alone, but total energy scaling is also not obeyed since the results for non-normal incidence are smaller than those for normal incidence.

For non-normal incidence, also the angular distribution of the scattered O_2 molecules that is shown in Fig. 10a has been analyzed in detail. The distribution shows that there is predominantly in-plane scattering, i.e. the molecules do not significantly change their azimuthal angle. In Fig. 10a, the results for the inplane scattering are compared to the experiment [85]. There is a rather good agreement between theory and experiment.

However, it is important to note that the angular distribution of Ar atoms scattered from Pt(111) is very similar to that of O_2 scattered at the same surface [86, 85]. The interaction potential of noble gas atoms with low-index metal surfaces is usually relatively structureless and only weakly corrugated. The similarity between Ar/Pt(111) and O_2/Pt(111) scattering indicates that also the O_2 scattering corresponds to the reflection from a rather flat surface. This has already been indicated by the weak out-of-plane scattering in the system O_2/Pt(111). The width of the in-plane distribution can in fact be explained by the energy transfer to a vibrating flat surface [85] which leads to a certain width in the distribution of the normal component of the kinetic energy. Together with the conservation of the parallel momentum of the scattered particles this causes the broadened angular distribution around the specular direction in the scattering.

Thus there is the seemingly paradox conclusion that adsorption experiments suggest that the O_2/Pt(111) interaction potential should be strongly corrugated while scattering experiments indicate a rather small corrugation. This contradiction is caused by the fact that the scattered molecules are reflected directly from the repulsive tails of the potential which is less strongly corrugated while in the trapping the corrugation and anisotropy of the potential energy surface closer to the surface become important.
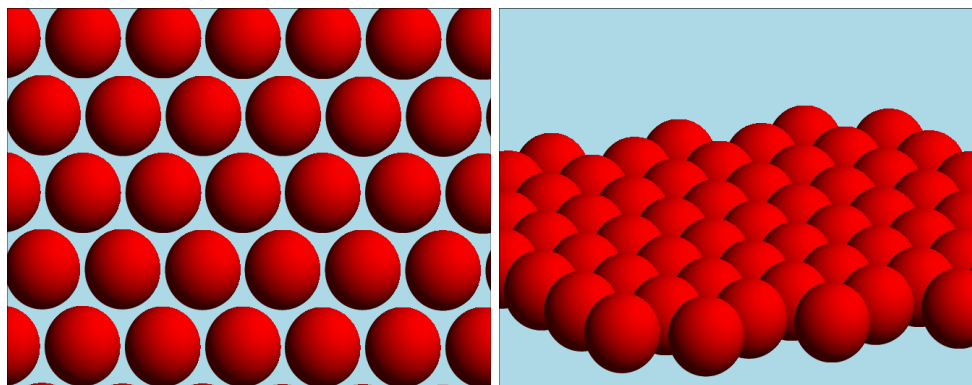
Figure 11: Illustration of the different apparent corrugation of a surface as a function of the angle of incidence.

This phenomenon is illustrated in Fig. 11. In the system $O_2/Pt(111)$ scattering corresponds to the majority channel at higher kinetic energies while adsorption is the minority channel. Adsorption is strongly dependent on the corrugation of the surface, however, for the scattered molecules at higher angles of incidence, due to shadowing effects the surface looks rather smooth. Since adsorption is the minority channel, the additional scattering flux which results from the suppression of adsorption at higher angles of incidence does not crucially influence the scattering distribution.

7   Conclusions

In this chapter, I have briefly reviewed the fundamentals of the dynamics of gas-surface interactions and their theoretical treatment. There are some phenomena in this interaction such as elastic scattering and diffraction that can only be understood in a quantum treatment. Most of the processes, however, can be understood qualitatively and even quantitatively based on classical dynamics simulations.

While atomic and molecular adsorption require a appropriate treatment of the excitation spectrum of the semi-infinite solid in order to correctly describe the energy transfer to the substrate, in the dissociative adsorption of light molecules, in particular H_2, this transfer can be neglected since the crucial process is the bond-breaking upon adsorption. However, a reliable high-dimensional potential energy surface is needed in order to reproduce the dependence of the adsorption probability on the internal degrees of freedom of the impinging molecules. *Ab initio* based molecular dynamics simulations are capable of giving a reliable and rather complete picture of the interaction of molecules with surfaces.

Electronically non-adiabatic processes have not been discussed in this chapter. Their theoretical treatment is still problematic. Such processes can either lead to further energy losses due to the excitation of electron-hole pairs in the substrate, or they modify the reaction dynamics due to transitions between electronically excited states. However, for most thermal processes at surfaces, electronically non-adiabatic processes only seem to play a minor role.

References

[1] A. Groß, Dynamics of molecule-surface interactions from first principles, in *The Chemical Physics of Solid Surfaces*, edited by D. P. Woodruff, volume 11, chapter 1, Elsevier, Amsterdam, 2003.

[2] A. Groß, Surf. Sci. Rep. **32**, 291 (1998).

[3] M. Born and J. R. Oppenheimer, Ann. Phys. **84**, 457 (1927).

[4] W. Kohn, Rev. Mod. Phys. **71**, 1253 (1999).

[5] W. H. Press, S. A. Teukolsky, W. T. Vetterling, and B. P. Flannery, *Numerical Recipes in Fortran 90. The Art of Parallel Scientific Computing*, Cambridge University Press, second edition, 1996.

[6] L. Verlet, Phys. Rev. **159**, 98 (1967).

[7] D. Heermann, *Computer Simulation Methods in Theoretical Physics*, Springer, Berlin, second edition, 1990.

[8] A. Groß, *Theoretical surface science – A microscopic perspective*, Springer, Berlin, 2002.

[9] R. Newton, *Scattering Theory of Waves and Particles*, Springer, New York, second edition, 1982.

[10] J. A. Fleck, J. R. Morris, and M. D. Feit, Appl. Phys. **10**, 129 (1976).

[11] M. D. Feit, J. A. Fleck, and A. Steiger, J. Comput. Phys. **47**, 412 (1982).

[12] H. Tal-Ezer and R. Kosloff, J. Chem. Phys. **81**, 3967 (1984).

[13] W. Brenig, T. Brunner, A. Groß, and R. Russ, Z. Phys. B **93**, 91 (1993).

[14] W. Brenig, , A. Groß, and R. Russ, Z. Phys. B **97**, 311 (1995).

[15] I. Estermann and O. Stern, Z. Phys. **61**, 95 (1930).

[16] E. Hulpke, editor, *Helium Atom Scattering from Surfaces*, volume 27 of *Springer Series in Surface Sciences*, Springer, Berlin, 1992.

[17] D. Farías and K.-H. Rieder, Rep. Prog. Phys. **61**, 1575 (1998).

[18] B. Gumhalter, Phys. Rep. **351**, 1 (2001).

[19] R. Frisch and O. Stern, Z. Phys. **84**, 430 (1933).

[20] M. Patting, D. Farías, and K.-H. Rieder, Surf. Sci. **429**, L503 (1999).

[21] R. G. Rowe and G. Ehrlich, J. Chem. Phys. , 4648 (1975).

[22] G. Brusdeylins and J. P. Toennies, Surf. Sci. **126**, 647 (1983).

[23] J. Lapujoulade, Y. Lecruer, M. Lefort, Y. Lejay, and E. Maurel, Surf. Sci. **103**, L85 (1981).

[24] M. F. Bertino and D. Farías, J. Phys.: Condens. Matter **14**, 6037 (2002).

[25] K. B. Whaley, C.-F. Yu, C. S. Hogg, J. C. Light, and S. Sibener, J. Chem. Phys. **83**, 4235 (1985).

[26] A. Groß and M. Scheffler, Chem. Phys. Lett. **263**, 567 (1996).

[27] U. Garibaldi, A. C. Levi, R. Spadacini, and G. E. Tommei, Surf. Sci. **48**, 649 (1995).

[28] M. F. Bertino, F. Hofmann, and J. P. Toennies, J. Chem. Phys. **106**, 4327 (1997).

[29] D. Cvetko, A. Morgante, A. Santaniello, and F. Tommasini, J. Chem. Phys. **104**, 7778 (1996).

[30] J. T. Kindt, J. C. Tully, M. Head-Gordon, and M. A. Gomez, J. Chem. Phys. **109**, 3629 (1998).

[31] E. K. Grimmelmann, J. C. Tully, and M. J. Cardillo, J. Chem. Phys. **72**, 1039 (1980).

[32] E. W. Kuipers, M. G. Tenner, M. E. M. Spruit, and A. W. Kleyn, Surf. Sci. **205**, 241 (1988).

[33] C. T. Rettner and C. B. Mullins, J. Chem. Phys. **94**, 1626 (1991).

[34] H. Schlichting, D. Menzel, T. Brunner, and W. Brenig, J. Chem. Phys. **97**, 4453 (1992).

[35] H. Schlichting, D. Menzel, T. Brunner, W. Brenig, and J. C. Tully, Phys. Rev. Lett. **60**, 2515 (1988).

[36] R. Sedlmeir and W. Brenig, Z. Phys. B **36**, 245 (1980).

[37] R. W. Fuller, S. M. Harris, and E. L. Slaggie, Am. J. Phys. **31**, 431 (1963).

[38] W. Brenig, Z. Phys. B **36**, 81 (1979).

[39] J. Böheim and W. Brenig, Z. Phys. B **41**, 243 (1981).

[40] G. B. Arfken and H. J. Weber, *Mathematical Methods for Physicists*, Academic Press, San Diego, 4th edition, 1995.

[41] W. Brenig, Z. Phys. B **36**, 227 (1980).

[42] I. A. Yu et al., Phys. Rev. Lett. **71**, 1589 (1993).

[43] S. Wilke and M. Scheffler, Phys. Rev. B **53**, 4926 (1996).

[44] S. Sakong and A. Groß, Surf. Sci., accepted for publication.

[45] K. D. Rendulic and A. Winkler, Surf. Sci. **299/300**, 261 (1994).

[46] G. R. Darling and S. Holloway, Rep. Prog. Phys. **58**, 1595 (1995).

[47] G.-J. Kroes, Prog. Surf. Sci. **60**, 1 (1999).

[48] W. Diño, H. Kasai, and A. Okiji, Prog. Surf. Sci. **63**, 63 (2000).

[49] A. Groß, S. Wilke, and M. Scheffler, Phys. Rev. Lett. **75**, 2718 (1995).

[50] G.-J. Kroes, E. J. Baerends, and R. C. Mowrey, Phys. Rev. Lett. **78**, 3583 (1997).

[51] K. D. Rendulic, G. Anger, and A. Winkler, Surf. Sci. **208**, 404 (1989).

[52] A. Eichler, J. Hafner, A. Groß, and M. Scheffler, Phys. Rev. B **59**, 13297 (1999).

[53] C. T. Rettner and D. J. Auerbach, Chem. Phys. Lett. **253**, 236 (1996).

[54] M. Beutl, M. Riedler, and K. D. Rendulic, Chem. Phys. Lett. **256**, 33 (1996).

[55] M. Gostein and G. O. Sitz, J. Chem. Phys. **106**, 7378 (1997).

[56] D. A. King, CRC Crit. Rev. Solid State Mater. Sci. **7**, 167 (1978).

[57] M. Kay, G. R. Darling, S. Holloway, J. A. White, and D. M. Bird, Chem. Phys. Lett. **245**, 311 (1995).

[58] A. Groß and M. Scheffler, J. Vac. Sci. Technol. A **15**, 1624 (1997).

[59] H. F. Busnengo, W. Dong, and A. Salin, Chem. Phys. Lett. **320**, 328 (2000).

[60] C. Crespos, H. F. Busnengo, W. Dong, and A. Salin, J. Chem. Phys. **114**, 10954 (2001).

[61] D. A. McCormack et al., Chem. Phys. Lett. **328**, 317 (2000).

[62] H. A. Michelsen and D. J. Auerbach, J. Chem. Phys. **94**, 7502 (1991).

[63] C. T. Rettner, D. J. Auerbach, and H. A. Michelsen, Phys. Rev. Lett. **68**, 1164 (1992).

[64] A. Groß, B. Hammer, M. Scheffler, and W. Brenig, Phys. Rev. Lett. **73**, 3121 (1994).

[65] D. A. McCormack and G.-J. Kroes, Phys. Chem. Chem. Phys. **1**, 1359 (1999).

[66] Y. Miura, H. Kasai, and W. Diño, J. Phys.: Condens. Matter **14**, L479 (2002).

[67] B. Hammer, M. Scheffler, K. Jacobsen, and J. Nørskov, Phys. Rev. Lett. **73**, 1400 (1994).

[68] J. A. White, D. M. Bird, M. C. Payne, and I. Stich, Phys. Rev. Lett. **73**, 1404 (1994).

[69] G. Wiesenekker, G.-J. Kroes, and E. J. Baerends, J. Chem. Phys. **104**, 7344 (1996).

[70] M. Karikorpi, S. Holloway, N. Henriksen, and J. K. Nørskov, Surf. Sci. **179**, L41 (1987).

[71] J. C. Polanyi and W. H. Wong, J. Chem. Phys. **51**, 1439 (1969).

[72] A. Groß and M. Scheffler, Chem. Phys. Lett. **256**, 417 (1996).

[73] W. Wurth et al., Phys. Rev. Lett. **65**, 2426 (1990).

[74] C. Puglia et al., Surf. Sci. **342**, 119 (1995).

[75] A. Eichler and J. Hafner, Phys. Rev. Lett. **79**, 4481 (1997).

[76] A. Eichler, F. Mittendorfer, and J. Hafner, Phys. Rev. B **62**, 4744 (2000).

[77] J. P. Perdew et al., Phys. Rev. B **46**, 6671 (1992).

[78] A. C. Luntz, M. D. Williams, and D. S. Bethune, J. Chem. Phys. **89**, 4381 (1988).

[79] P. D. Nolan, B. R. Lutz, P. L. Tanaka, J. E. Davis, and C. B. Mullins, J. Chem. Phys. **111**, 3696 (1999).

[80] P. D. Nolan, B. R. Lutz, P. L. Tanaka, J. E. Davis, and C. B. Mullins, Phys. Rev. Lett. **81**, 3179 (1998).

[81] A. Groß, M. Bockstedte, and M. Scheffler, Phys. Rev. Lett. **79**, 701 (1997).

[82] A. Groß, M. Scheffler, M. J. Mehl, and D. A. Papaconstantopoulos, Phys. Rev. Lett. **82**, 1209 (1999).

[83] A. Groß, A. Eichler, J. Hafner, M. J. Mehl, and D. A. Papaconstantopoulos, Surf. Sci. **539**, L542 (2003).

[84] M. J. Mehl and D. A. Papaconstantopoulos, Phys. Rev. B **54**, 4519 (1996).

[85] A. E. Wiskerke, F. H. Geuzebroek, A. W. Kleyn, and B. E. Hayden, Surf. Sci. **272**, 256 (1992).

[86] J. E. Hurst, L. Wharton, K. C. Janda, and D. J. Auerbach, J. Chem. Phys. **78**, 1559 (1983).